Inorganic Chemistry

pubs.acs.org/IC

Article

$AInSn_2S_6$ (A = K, Rb, Cs)—Layered Semiconductors Based on the SnS_2 Structure

Daniel Friedrich, Michael A. Quintero, Shiqiang Hao, Craig C. Laing, Christopher Wolverton, and Mercouri G. Kanatzidis*

Cite This: *Inorg. Chem.* 2022, 61, 13525−13531

Read Online

ACCESS | Metrics & More | Article Recommendations | Supporting Information

ABSTRACT: $RbInSn_2S_6$ and $CsInSn_2S_6$ are yellow two-dimensional (2D) semiconductors featuring anionic SnS_2-type layers of edge-sharing $(In/Sn)S_6$ octahedra. These structures are directly derived from the parent structure of SnS_2 by replacement of Sn^{4+} atoms with A^+ and In^{3+} atoms. The compounds crystallize, isotypic to the ion-exchange material $KInSn_2S_6$. They adopt the triclinic space group $R\bar{3}m$ (no. 166). The compounds have similar indirect optical band gaps of 2.31(5) eV for Rb and 2.47(5) eV Cs. The measured work functions for each material are ∼5.38 eV. The density functional theory-calculated effective mass values exhibit strong anisotropy due to the 2D nature of the crystal structures and in the case of $CsInSn_2S_6$ for hole carriers along the a, b, and c crystallographic directions are 0.30 m_0, 0.34 m_0, and 2.54 m_0, respectively, while for electrons are 0.06 m_0, 0.07 m_0, and 0.47 m_0, respectively.

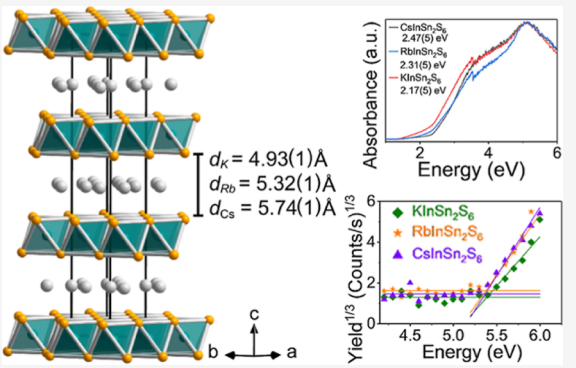

INTRODUCTION

Multinary chalcogenide semiconductors are multifunctional materials with diverse chemical and physical properties and are promising for various technological applications. Among this class of solids, quaternary chalcogenide materials $A_aM_bM_c'Q_d$ (A = alkali metal, thallium; M = group 13 metal; M' = group 14 metal; Q = chalcogen) feature a covalently bonded anionic framework of $[M_bM_c'Q_d]^{a-}$ of any dimensionality, that is, one-dimensional (1D), two-dimensional (2D), or three-dimensional (3D), and charge balancing alkali cations.[1−7] Prominent examples of these properties are the strong nonlinear optical (NLO) second-harmonic generation (SHG) of noncentrosymmetric materials such as $LiGaGe_2Q_6$,[8−11] $A_2In_2M'Q_6$,[12−16] and $TlGaSn_2Q_6$.[17−22] A series of centrosymmetric $AGaM'Q_4$ (A = K, Rb, Cs, Tl; M' = Si; Ge, Sn; Q = S, Se) polymorphs were reported to exhibit a high NLO third-harmonic generation scaling inversely with their band gaps following a power-law behavior.[2,3,14,15,23−25] Among 3D quaternary chalcogenides, the chalcopyrite materials such as $Cu(In,Ga)Se_2$, $Cu(In,Ga)(S, Se)_2$, and Cu_2ZnSnS_4 are currently of great interest as promising photovoltaics.[26−28] While the covalent anionic frameworks have optoelectronic functionalities depending on their composition and structure, the alkali metal counterions also represent chemical functionality because they often can be exchanged for other cations, thereby modifying the chemical composition. The so-called KMS family is a special subclass with a layered structure and remarkable ion-exchange properties relevant to environmental remediation.[7,29−36] This family is defined as $A_x[M_xSn_{3-x}S_6]$, M being a divalent or trivalent metal.[37] These structures are directly related to SnS_2 and can be derived from a fivefold super cell by symmetry transformations. $KInSn_2S_6$ is a member of this family capable of fast ion exchange with trivalent lanthanide and actinide cations, promising for treating radioactive wastewater.[7] In this work, we present the synthesis and physical characterization of the analogous $RbInSn_2S_6$ and $CsInSn_2S_6$, crystallizing isotypic to $KInSn_2S_6$.[7] The crystal structures of these compounds feature anionic layers of edge-sharing $(In/Sn)S_6$ octahedra similar to that in layered SnS_2. Their electronic structures have been analyzed by complementary density functional theory (DFT) calculations. All three 2D sulfides have similar indirect optical band gaps of 2.2−2.5 eV and feature identical work functions within error.

EXPERIMENTAL SECTION

Starting Materials. Commercially available elements potassium (K, Sigma-Aldrich, 99.95%), rubidium (Rb, Alfa Aesar, 99.5%), cesium (Cs, Alfa Aesar, 99.5%), indium (In, Chempur, 99.999%), tin (Sn, American Elements, 99.99%), and sulfur (S, 5 N Plus, 99.999%) were used as purchased without further purification. The alkali metal chalcogenides A_2Q (A = K, Rb, Cs; Q = S, Se) were prepared by

Received: June 22, 2022
Published: August 12, 2022

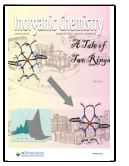

https://doi.org/10.1021/acs.inorgchem.2c02157
Inorg. Chem. 2022, 61, 13525−13531

Table 1. Crystallographic Data[a] of $AInSn_2S_6$ (A = K, Rb, Cs)

compound	$KInSn_2S_6$ (1)	$RbInSn_2S_6$ (2)	$CsInSn_2S_6$ (3)
formula weight M/g·mol^{-1}	583.66	630.03	677.42
color/shape		yellow plate	
crystal system, space group		trigonal, $R\bar{3}m$ (no. 166)	
lattice parameters			
a/Å	3.693(1)	3.693(1)	3.690(1)
c/Å	23.466(3)	24.667(7)	25.910(9)
unit cell volume V/Å^3	277.1(1)	291.3(2)	305.6(2)
number of formula units Z		1	
calculated density ρ/g·cm^{-3}	3.498	3.591	3.681
diffractometer		Bruker Kappa Apex II	
temperature T/°C		20	
wavelength λ/Å		0.71073	
absorption coeff. μ(Mo Kα)/mm^{-1}	7.973	11.376	9.825
θ range/°	2.604−26.550	2.477−26.293	2.358−26.150
index range	$-4 \le h \le 3$	$-4 \le h \le 4$	$-4 \le h \le 4$
	$-4 \le k \le 4$	$-4 \le k \le 4$	$-4 \le k \le 4$
	$-28 \le l \le 28$	$-29 \le l \le 30$	$-23 \le l \le 31$
no. of reflections collected	1519	1431	280
Independent reflections	96	102	105
R_{int}, R_σ	0.0300, 0.0115	0.0402, 0.0154	0.0188, 0.0129
completeness to θ = 25°		99.9%	
absorption correction		numerical (analytical, based on crystal faces), APEX3	
structure solution		intrinsic phasing, ShelXT	
structure refinement		ShelXL, full-matrix least-squares on F^2	
data/restraints/parameters	96/0/10	102/0/10	105/0/10
GooF, F(000)	1.175, 264	1.277, 282	1.266, 300
R_1, wR_2 [$I > 3\sigma(I)$]	0.0111, 0.0265	0.0139, 0.0313	0.0308, 0.0790
R_1, wR_2 [all data]	0.0111, 0.0265	0.0139, 0.0313	0.0319, 0.0805
extinction coefficient G_{iso}		0.0039(8)	
largest diff. peak and hole/e·Å^{-3}	−0.357, 0.554	−0.355, 0.966	−0.648, 1.577

[a]Further details on the crystal structure investigations may be obtained from Fachinformationszentrum Karlsruhe, 76344 Eggenstein-Leopoldshafen, Germany (fax: (+49)7247-808-666; E-mail: crysdata@fiz-karlsruhe.de), on quoting the depository number CSD-2179423 for $KInSnS_2S_6$, CSD-2179424 for $RbInSnS_2S_6$, and CSD-2179422 for $CsInSnS_2S_6$.

reacting the alkali metals with the respective chalcogens in liquid ammonia.[4] SnS_2 was prepared by annealing a stoichiometric mixture of Sn and S in an evacuated quartz tube at 550 °C for 3 days. In_2S_3 was prepared by combining stoichiometric amounts of Sn and S in a fused silica tube, evacuating to ∼5 × 10^{-3} mbar, flame sealing, and heating to 600 °C at a rate of 50°/h, where the tube was annealed for 30 min, after which it was cooled to room temperature.

Synthesis of the Title Compounds. *Method 1.* The $AInSn_2S_6$ compounds (A = K, Rb, Cs) were prepared by a high-temperature solid-state reaction of stoichiometric amounts of the respective starting materials in evacuated fused silica tubes. In a typical batch of 1.0 g, stoichiometric amounts of A_2S and other precursor materials were weighed in a fused silica tube (an inner diameter of 8 mm) in a nitrogen-filled glovebox. For $KInSn_2S_6$ (1), 0.0944 g (0.85 mmol) of K_2S, 0.1967 g (1.71 mmol) of In, 0.4067 g (3.43 mmol) of Sn, and 0.3021 g (9.42 mmol) of S were used. $RbInSn_2S_6$ (2) was obtained by combining 0.1611 g (0.79 mmol) of Rb_2S, 0.1822 g (1.58 mmol) of In, 0.3768 g (3.17 mmol) of Sn, and 0.2799 g (8.73 mmol) of S. For the synthesis of $CsInSn_2S_6$ (3), 0.2198 g (0.74 mmol) of Cs_2S, 0.1695 g (1.48 mmol) of In, 0.3504 g (2.95 mmol) of Sn, and 0.2603 g (8.12 mmol) of S were used. The tubes containing the starting mixtures were evacuated to ∼10^{-4} mbar, flame-sealed to 10−11 cm long tubes, and placed in a programmable furnace. The samples were heated to 800 °C with a heating rate of 1 °C/min, annealed at 800 °C for 24 h, and cooled to room temperature at a cooling rate of 1 °C/min. All tubes contained a soft, yellow, sintered polycrystalline material that could easily be crushed in an agate mortar while falling apart into plate-like crystallites. The phase purity and crystallinity of the solid products were determined by powder X-ray diffraction (PXRD) techniques after the opening of the tubes, and the chemical composition was verified by scanning electron microscopy/energy-dispersive system (EDS) analyses of several crystallites (Figure S2). All samples were single-phase solids unless stated otherwise. The powdered solids are stable in moist air.

Method 2. The $AInSn_2S_6$ compounds (A = K, Rb, Cs) can be equivalently prepared below their respective melting points. In a typical batch of 1.0 g, stoichiometric amounts of A_2S, the Sn powder, S buttons, and the In_2S_3 powder were massed in a nitrogen-filled glovebox. For $KInSn_2S_6$ (1), 0.0944 g (0.85 mmol) of K_2S, 0.2791 g (0.85 mmol) of In_2S_3, 0.4067 g (3.43 mmol) of Sn, and 0.2197 g (6.85 mmol) of S were used. $RbInSn_2S_6$ (2) was obtained by combining 0.1611 g (0.79 mmol) of Rb_2S, 0.2586 g (0.79 mmol) of In_2S_3, 0.3768 g (3.17 mmol) of Sn, and 0.2036 g (6.35 mmol) of S. For the synthesis of $CsInSn_2S_6$ (3), 0.2198 g (0.74 mmol) of Cs_2S, 0.2405 g (0.74 mmol) of In_2S_3, 0.3504 g (2.95 mmol) of Sn, and 0.1893 g (5.90 mmol) of S were used. The above amounts were ground together in an agate mortar and pestle until homogeneous. The resultant mixture was loaded into 8 mm inner diameter, 10 mm outer diameter fused silica tubes that were internally lined with an Al foil. The Al foil is necessary to protect the region to be sealed from the powder; without its use, the reactant residue on the glass will react with silica in the high heat of the torch, producing high-melting-point silicates in the sealing region, making effective sealing of the ampule difficult. After loading, the Al foil was removed, and the tubes were evacuated to ∼10^{-4} mbar, flame-sealed to 10−11 cm long tubes, and placed in a programmable tube furnace. The samples were heated to 700 °C at a heating rate of 50 °C/h and annealed at 700 °C for 24 h,

https://doi.org/10.1021/acs.inorgchem.2c02157
Inorg. Chem. 2022, 61, 13525−13531

after which the furnace was turned off, and the samples were allowed to cool to room temperature.

Powder X-ray Diffraction. PXRD patterns were collected on a Rigaku Miniflex600 diffractometer using Cu Kα1 radiation (λ = 1.540593 Å) equipped with a high-speed silicon strip detector. Finely powdered samples were measured on a flat zero-background Si sample. The experimental patterns were compared to simulated patterns based on the experimental CIF files.

Single-Crystal X-ray Diffraction. Plate-shaped single crystals of the title compounds were selected under a polarizing microscope in order to find suitable crystals without stacking faults. The selected crystals were fixed to MiTeGen mounts using silicon grease, and ambient temperature diffraction data were collected on a Bruker Kappa APEX II diffractometer equipped with an IμS microfocus X-ray (Mo Kα radiation, λ = 0.71073 Å) source and an APEX2 charge-coupled detector. The resulting diffraction data were corrected for Lorentz and polarization effects, and the absorption was corrected by a numerical absorption correction (based on the crystal faces) using the Bruker APEX II software suite.[38] All collected data sets had a completeness of 99.9% within 50° 2θ. The crystal structures were solved by intrinsic phasing methods using ShelXT2018/3[39] and refined on F^2 with ShelXL2018/3[38] using full-matrix least-squares methods. As In^{3+} and Sn^{4+} cannot be distinguished using conventional X-ray diffraction techniques, the occupation factors were set to 33 and 66%, respectively, to ensure charge-balanced structures. The resulting structure models were checked for missed symmetry and transformed into the standard setting using the PLATON software package.[40]

UV−Vis Diffuse Reflectance Spectroscopy. Optical diffuse reflectance measurements were performed at room temperature using a Cary 5000 UV−Vis−NIR double-monochromator spectrophotometer operating from 200 to 2500 nm. $BaSO_4$ was used as a nonabsorbing reflectance reference. The generated reflectance data were transformed to absorbance via the Kubelka−Munk equation[41] $\alpha/S = (1 - R)^2/2R$, where R is the reflectance and α and S are the absorption and scattering coefficients, respectively. The absorption edge was estimated by extrapolation of the linear regions.

DFT Calculations. DFT calculations within the generalized gradient approximation (GGA) were used to calculate the electronic structures of the title compounds.[42] To yield a band gap with an accuracy similar to that of the hybrid functional or GW methods and make it computationally less expensive, we adopted a kind of local approximation named the modified Becke−Johnson exchange potential.[43,44] The periodic boundary conditions and a plane-wave basis set were utilized as implemented in the Vienna Ab initio Simulation package.[45] The total energies were numerically converged to approximately 3 meV/cation using a basis set energy cutoff of 500 eV and dense k-meshes corresponding to 4000 k-points per reciprocal atom in the Brillouin zone. In order to find proper structure models for the mixed In−Sn occupation, the lowest energy configuration was chosen from a vast number of geometrical structures. For the five structures with the lowest electrostatic energies, further DFT calculations were performed to identify the most favorable (lowest energy) configuration.

RESULTS AND DISCUSSION

Crystal Structure Discussion. The crystal structures of the new compounds $A\mathrm{InSn_2S_6}$ (A = Rb, Cs) (**2, 3**) were solved from X-ray single-crystal data and crystallized from the previously reported $\mathrm{KInSn_2S_6}$ structure. The potassium analogue was also remeasured for the sake of completeness and comparison of these structures. These solids crystallize in the trigonal space group $R\bar{3}m$ (no. 166) with unit cell parameters of a = 3.69(1) Å and c = 23.5(1)−25.9(1) Å. Details on the data collection are given in Table 1. The atomic coordinates of compounds **1−3** are given in Table 2. The anisotropic displacement parameters and interatomic distances are given in Tables S1−S6 of the Supporting Information.

Table 2. Atomic Coordinates and Isotropic Displacement Parameters U_{eq}/Å^2 for $A\mathrm{InSn_2S_6}$ (A = K, Rb, Cs; T = 20 °C)

atom	wyck.	s.o.f.	x	y	z	U_{eq}[a]
K	6c	0.167	0	0	0.1667(2)	0.043(2)
In	3a	0.333	0	0	0	0.015(1)
Sn	3a	0.667	0	0	0	0.015(1)
S	6c	1	0	0	0.3951(1)	0.015(1)
Rb	6c	0.167	0	0	0.1666(2)	0.050(1)
In	3a	0.333	0	0	0	0.015(1)
Sn	3a	0.667	0	0	0	0.015(1)
S	6c	1	0	0	0.3922(1)	0.016(1)
Rb	6c	0.167	0	0	0.1665(2)	0.071(2)
In	3a	0.333	0	0	0	0.021(1)
Sn	3a	0.667	0	0	0	0.021(1)
S	6c	1	0	0	0.3892(1)	0.021(1)

[a] U_{eq} is defined as the trace of one-third of the U_{ij} tensors.

The structure of the three isotypic compounds $A\mathrm{InSn_2S_6}$ (**1−3**) (A = K, Rb, Cs) features anionic layers of edge-sharing $(\mathrm{In/Sn})S_6$ octahedra separated by the alkali metal cations as seen in Figure 1a. The In^{3+} and Sn^{4+} cations occupy one

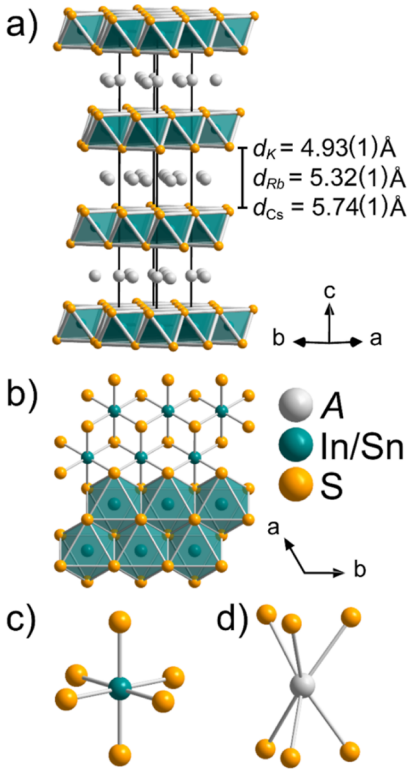

Figure 1. Crystal structure of the $A\mathrm{InSn_2S_6}$ compounds, showing (a) the unit cell of $A\mathrm{InSn_2S_6}$ (note that the alkali metal sites are only occupied by 16.6%). (b) Section of one anionic $^2_\infty[\mathrm{InSn_2S_6^-}]$ layer. (c) Coordination environment of the In/Sn site. (d) Coordination environment of the alkali metal site.

crystallographically independent 3a special site with occupation factors of 33.3 and 66.7%, respectively. The cations are in an octahedral environment with six identical distances d(In/Sn−S) = 2.577(2) Å (Figure 1c) observed in all three compounds. These bond distances align perfectly with the sum of the ionic radii $d(\mathrm{In^{3+}\text{-}S^{2-}})$ = 2.64 Å and $d(\mathrm{Sn^{4+}\text{-}S^{2-}})$ = 2.53 Å under the assumption that the site is occupied by 2/3 Sn^{4+}

https://doi.org/10.1021/acs.inorgchem.2c02157
Inorg. Chem. 2022, 61, 13525−13531

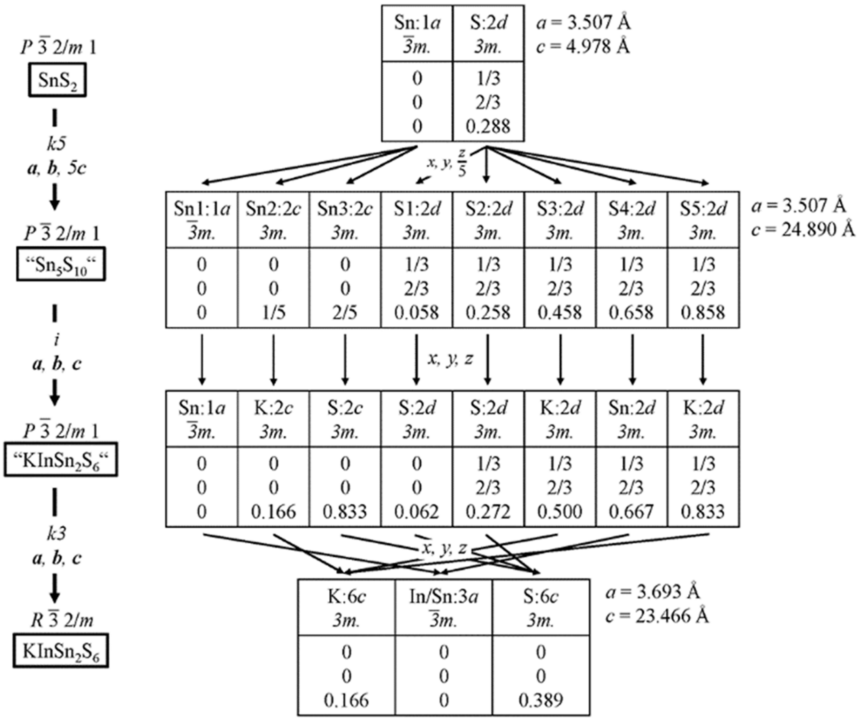

Figure 2. Bärnighausen tree explaining the symmetry relations between the structures of SnS_2 ($P\bar{3}m$) and $KInSn_2S_6$ ($R\bar{3}m$) as an example of the $AInSn_2S_6$ compounds.

and 1/3 In^{3+}, respectively.[46] The axial angles in these octahedra are 180°, and the equatorial angles only differ from the ideal value of 90° by ∼1.5° (slightly more than the difference of 0.3° observed in SnS_2), making these octahedra the almost ideal octahedra. The In/SnS_6 octahedra are connected by six common edges, forming anionic layers $^{2}_{\infty}[InSn_2S_6^-]$ which are also observed in SnS_2 (Figure 1b). The alkali metal cations occupy one common 6*c* site with a 16.6% occupation factor and are in a trigonal prismatic coordination formed by six S^{2-} anions (Figure 1d). In $KInSn_2S_6$, six identical distances d(K−S) = 3.257(4) Å are observed, while the cesium and rubidium analogues exhibit two marginally different distances of d(Rb−S) = 3.408(3) Å, d(Rb−S) = 3.411(3) Å, d(Cs−S) = 3.573(5) Å, and d(Cs−S) = 3.579(5) Å, respectively. These values are only slightly higher than the sum of the ionic radii of $d(K^+\text{-}S^{2-})$ = 3.22 Å, $d(Rb^+\text{-}S^{2-})$ = 3.36 Å, and $d(Cs^+\text{-}S^{2-})$ = 3.51 Å.[46]

The alkali metal cations are located between the anionic layers with almost identical distances of $d(A-A) \approx 3.690(3)$ Å in all three $AInSn_2S_6$ compounds. The van der Waals distances between two anionic layers are 4.925(1) Å ($KInSn_2S_6$), 5.320(2) Å ($RbInSn_2S_6$), and 5.744(4) Å ($CsInSn_2S_6$). Due to the alkali intercalation in between the chalcogenide layers, these distances are roughly twice as large as those in the parent structure SnS_2 with ∼2.8 Å.

The layered structure of $AInSn_2S_6$ does not only show layers identical to the parent structure SnS_2; both structures are directly related and can be converted into each other by symmetry relations. Figure 2 shows a Bärnighausen tree explaining these relations. $AInSn_2S_6$ crystallizes in the space group $R\bar{m}$ (no. 166) which is a supergroup of $P\bar{m}$ (no. 164), the space group of SnS_2, related by a *klassengleiche* transformation of index 3. This change can also be observed by comparing the PXRD patterns of the structures with $AInSn_2S_6$ (A = K, Rb, Cs) only showing 003*l* reflections compared to the 00*l* reflections in SnS_2. Before transforming the structures, however, the unit cell of SnS_2 needs to be enlarged fivefold by applying a *klassengleiche* transformation of index 5, multiplying the *c*-axis by 5, and dividing all *z* coordinates by 5. Consequently, the Sn 1*a* site is split into one 1*a* and two 2*c* sites, while the S 2*d* site is divided into five 2*d* sites. To transform the expanded structure of SnS_2 into the structure of $AInSn_2S_6$, the atoms occupying these sites are shuffled. The 1*a* Sn site retains Sn^{4+} cations, while the 2*c* Sn sites are occupied by A^+ and S^{2-}, respectively. Two of the five 2*d* S sites are occupied by K^+ and one by Sn^{4+} cations instead of S^{2-} anions. Minor differences of the actual values of the *z* coordinates are attributed to the influence of the alkali metal cations contracting or expanding the distance between the anionic layers.

The thermal properties of $AInSn_2S_6$ (A = K, Rb, Cs) are shown in Figure S3a−c. The differential thermal analysis (DTA) curves of each material show one prominent thermal event attributed to melting in their heating curves at ∼743 °C for $KInSn_2S_6$, ∼735 °C for $RbInSn_2S_6$, and ∼726 °C for $CsInSn_2S_6$. As the identity of the alkali metal is exchanged from K → Rb → Cs, a small decrease in the melting point of the compounds is observed. This trend makes sense as Cs−S bonds are weaker than Rb−S bonds, which are weaker than K−S bonds and can be intuited from the general observed trend in the melting points of the A_2S_x binaries when comparing compounds with identical x values. Comparisons between PXRD patterns taken both before and after the DTA, see Figure S3d−f, suggest that the compounds melt congruently as the patterns do not change appreciably. For both $KInSn_2S_6$ and $RbInSn_2S_6$, at least one or more secondary phases can be observed in their PXRD patterns both before and after being heated. The relative amounts of these phases do not appear to change substantially after two heating cycles.

https://doi.org/10.1021/acs.inorgchem.2c02157
Inorg. Chem. 2022, 61, 13525−13531

These observations in conjunction with the lack of any other observed thermal events other than the main melting and solidification events support the conclusion that both compounds melt congruently.

Electronic Structure and Optical Properties. The optical absorption data for compounds **1**−**3** obtained from diffuse reflectance measurements are shown in Figure 3a. The

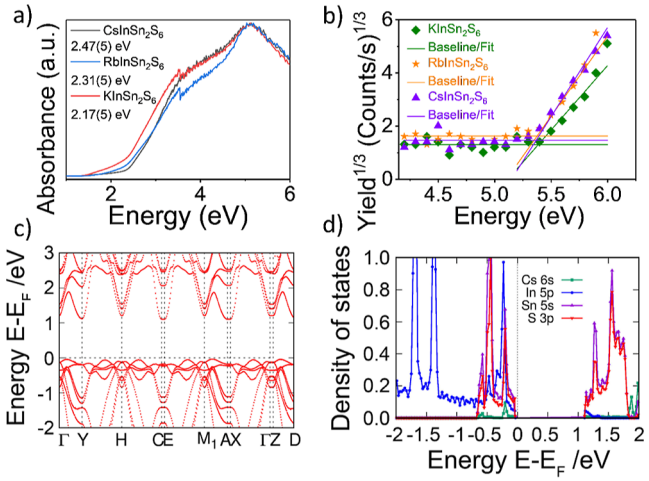

Figure 3. (a) UV−vis absorption spectra and (b) PYSA of $A\mathrm{InSn_2S_6}$ (**1**−**3**). (c) Band structure and (d) DOS plots of $\mathrm{CsInSn_2S_6}$ as a representative of the $A\mathrm{InSn_2S_6}$ phases (A = K, Rb, Cs).

observed optical band gaps are 2.17(5) eV for $\mathrm{KInSn_2S_6}$, 2.31(5) eV for $\mathrm{RbInSn_2S_6}$, and 2.47(5) eV for $\mathrm{CsInSn_2S_6}$. These compare well with the band gap of SnS_2, ∼2.17 eV, as the alkali metals do not contribute considerably to the states near the Fermi level in these and related compounds.[1,47−51] The trend of an increasing band gap upon substitution with larger alkali metals is reasonable and a consequence of the increased dimensional reduction coming from a larger interlayer separation. The increased interlayer distances lower the overall extent of bonding which results in a blue shift, or widening, of the band gap in a material.[52,53] Figure 3b shows the photoemission yield spectrum in air (PYSA) for compounds (**1**−**3**). The extrapolated x-intercept of the plot corresponds to the work function of a given material. It will thus be sensitive to any changes in the valence band that arise as a function of chemical substitution. The extrapolated work function for $\mathrm{KInSn_2S_6}$ is 5.37(2) eV, for $\mathrm{RbInSn_2S_6}$ is 5.39(2) eV, and for $\mathrm{CsInSn_2S_6}$ is 5.38(2) eV. The work functions for all materials in the series are identical within error, as expected, due to there being no substantial change in the orbital contributions of the valence band upon substitution. With the work function and the optical band gap in hand, the conduction band minimums can be derived relative to the vacuum energy according to the following relation: $E_{CBM} = E_{WF} - E_g$. The conduction band minimums of each material are then 3.20(5) eV for $\mathrm{KInSn_2S_6}$, 3.08(5) eV for $\mathrm{RbInSn_2S_6}$, and 2.91(5) eV for $\mathrm{CsInSn_2S_6}$. These values indicate that the blue shift observed in the band gaps for these materials is entirely caused by the movement of the conduction band minima toward lower values (i.e., closer to the vacuum energy).

To gain further insights into the electronic structures of these materials, complementary DFT calculations were performed. Standard DFT calculations using the GGA[45] always resulted in metallic structures with no band gaps. In order to yield more precise electronic structures of these semiconductors, a modified Becke−Johnson exchange potential was used, giving accuracy similar to that of hybrid functionals or GW methods.[43,44] These more elaborate calculations revealed the semiconducting nature of these materials, with the calculated band gaps being underestimated, as is expected from such DFT calculations due to the insufficient description of the electronic states when using the GGA. The $A\mathrm{InSn_2S_6}$ compounds (**1**−**3**) are indirect band gap semiconductors (Figure 3c), with the states below the Fermi level being dominated by the In-5p, Sn-5s, and S-3p states (Figure 3d). Contributions of the Sn-5p and S-3p states dominate the lowest states in the conduction band. The alkali metal s-states (K-3s, Rb-4s, and Cs-5s) have no significant contributions to the states close to the Fermi level as they are usually located below −8 eV.

In addition to the band structures, the effective masses of the electrons and holes for $\mathrm{CsInSn_2S_6}$ were calculated as a representative of these phases. Because of the 2D nature of the crystalline structure, the effective mass also exhibits strong anisotropic properties. For the holes, the effective mass along a, b, and c directions is, respectively, 0.30 m_0, 0.34 m_0, and 2.54 m_0. The larger value along the c-axis reflects the 2D nature of the system. For the electrons, the corresponding effective mass along a, b, and c directions is significantly smaller at 0.06 m_0, 0.07 m_0, and 0.47 m_0, respectively. Here, the low values for both holes and electrons in the in-plane directions are strikingly low, especially for the electrons. This implies that the charge carriers are expected to move with high mobilities within the layers. Interestingly, while the holes will have poor transport properties perpendicular to the layers because of the very heavy mass of 2.54 m_0, the electron mass along the same direction is surprisingly low at 0.47 m_0 and suggests an improved and rather fast electron flow along the c direction. For the density of states (DOSs) effective mass, defined as $m_d^* = (g^2 \cdot m_{kx} \cdot m_{ky} \cdot m_{kz})^{1/3}$, the resulting values of $m_e^* = 0.12\ m_0$ and $m_h^* = 0.63\ m_0$ are within expected values for this kind of structure. These low values indicate that these layered 2D chalcogenides are potentially very attractive regarding their electronic transport properties.

CONCLUSIONS

$\mathrm{RbInSn_2S_6}$ and $\mathrm{CsInSn_2S_6}$, two new quaternary 2D layered semiconductors in the KMS family, were prepared by solid-state synthesis and structurally characterized. They crystallize isotypic to the previously reported $\mathrm{KInSn_2S_6}$[7] and feature anionic layers of edge-sharing $\mathrm{In/SnS_6}$ octahedra. The crystal structures of these compounds are directly related to the layered structure of SnS_2 and can be derived from a fivefold supercell of the SnS_2 structure by symmetry transformations. These yellow semiconductors have indirect optical band gaps similar to their parent structure, SnS_2, and are expected to exhibit good charge transport properties in addition to the already demonstrated excellent ion-exchange properties of the KMS family.

ASSOCIATED CONTENT

Supporting Information

The Supporting Information is available free of charge at https://pubs.acs.org/doi/10.1021/acs.inorgchem.2c02157.

https://doi.org/10.1021/acs.inorgchem.2c02157
Inorg. Chem. 2022, 61, 13525−13531

PXRD patterns of compounds **1**−**3**; EDS spectra of compounds **1**−**3**; anisotropic displacement parameters and selected interatomic distances of compounds **1**−**3**; DTA curves of compounds **1**−**3**; and pre- and post-DTA PXRD patterns of compounds 1−3 (PDF)

Accession Codes

CCDC 2179422−2179424 contain the supplementary crystallographic data for this paper. These data can be obtained free of charge via www.ccdc.cam.ac.uk/data_request/cif, or by emailing data_request@ccdc.cam.ac.uk, or by contacting The Cambridge Crystallographic Data Centre, 12 Union Road, Cambridge CB2 1EZ, UK; fax: +44 1223 336033.

AUTHOR INFORMATION

Corresponding Author

Mercouri G. Kanatzidis − *Department of Chemistry, Northwestern University, Evanston, Illinois 60208, United States;* orcid.org/0000-0003-2037-4168; Email: m-kanatzidis@northwestern.edu

Authors

Daniel Friedrich − *Department of Chemistry, Northwestern University, Evanston, Illinois 60208, United States;* orcid.org/0000-0001-6953-8114

Michael A. Quintero − *Department of Chemistry, Northwestern University, Evanston, Illinois 60208, United States;* orcid.org/0000-0002-0709-1676

Shiqiang Hao − *Department of Materials Science and Engineering, Northwestern University, Evanston, Illinois 60208, United States;* orcid.org/0000-0002-7985-4468

Craig C. Laing − *Department of Chemistry, Northwestern University, Evanston, Illinois 60208, United States;* orcid.org/0000-0002-0654-4741

Christopher Wolverton − *Department of Materials Science and Engineering, Northwestern University, Evanston, Illinois 60208, United States;* orcid.org/0000-0003-2248-474X

Complete contact information is available at: https://pubs.acs.org/10.1021/acs.inorgchem.2c02157

Author Contributions

The manuscript was written through contributions of all authors. All authors have given approval to the final version of the manuscript.

Notes

The authors declare no competing financial interest.

ACKNOWLEDGMENTS

This synthesis and material characterization study was supported in part by the National Science Foundation through grant DMR-2003476. This study used the IMSERC facility at Northwestern University, which has received support from the Soft and Hybrid Nanotechnology Experimental (SHyNE) Resource (NSF ECCS-1542205), the State of Illinois, and the IIN. This study used the EPIC facility of Northwestern University's NUANCE Center, which has received support from the SHyNE Resource (NSF ECCS-2025633), the IIN, and the Northwestern MRSEC program (NSF DMR-1720139). D.F. thanks the German Research Foundation (DFG) for a fellowship (FR 4094/1−1).

REFERENCES

(1) Friedrich, D.; Byun, H. R.; Hao, S.; Patel, S.; Wolverton, C.; Jang, J. I.; Kanatzidis, M. G. Layered and Cubic Semiconductors $AGaM'Q_4$ ($A^+ = K^+, Rb^+, Cs^+, Tl^+$; $M'^{4+} = Ge^{4+}, Sn^{4+}$; $Q^{2-} = S^{2-}, Se^{2-}$) and High Third-Harmonic Generation. *J. Am. Chem. Soc.* **2020**, *142*, 17730−17742.

(2) Hwang, S.-J.; Iyer, R. G.; Kanatzidis, M. G. Quaternary selenostannates $Na_{2-x}Ga_{2-x}Sn_{1+x}Se_6$ and $AGaSnSe_4$ (A = K, Rb, and Cs) through rapid cooling of melts. Kinetics versus thermodynamics in the polymorphism of $AGaSnSe_4$. *J. Solid State Chem.* **2004**, *177*, 3640−3649.

(3) Hwang, S.-J.; Iyer, R. G.; Trikalitis, P. N.; Ogden, A. G.; Kanatzidis, M. G. Cooling of Melts: Kinetic Stabilization and Polymorphic Transitions in the $KInSnSe_4$ System. *Inorg. Chem.* **2004**, *43*, 2237−2239.

(4) Liao, J. H.; Varotsis, C.; Kanatzidis, M. G. Syntheses, structures, and properties of six novel alkali metal tin sulfides: $K_2Sn_2S_8$, alpha-$Rb_2Sn_2S_8$, beta-$Rb_2Sn_2S_8$, $K_2Sn_2S_5$, $Cs_2Sn_2S_6$, and Cs_2SnS_{14}. *Inorg. Chem.* **1993**, *32*, 2453−2462.

(5) Marking, G. A.; Hanko, J. A.; Kanatzidis, M. G. New quaternary thiostannates and thiogermanates $A_2Hg_3M_2S_8$ (A = Cs, Rb; M = Sn, Ge) through molten A_2S_x. Reversible glass formation in $Cs_2Hg_3M_2S_8$. *Chem. Mater.* **1998**, *10*, 1191−1199.

(6) Palchilk, O.; Marking, G. M.; Kanatzidis, M. G. Exploratory synthesis in molten salts: Role of flux basicity in the stabilization of the complex thiogermanates $Cs_4Pb_4Ge_5S_{16}$, $K_2PbGe_2S_6$, and $K_4Sn_3Ge_3S_{14}$. *Inorg. Chem.* **2005**, *44*, 4151−4153.

(7) Xiao, C. L.; Hassanzadeh Fard, Z. H.; Sarma, D.; Song, T. B.; Xu, C.; Kanatzidis, M. G. Highly Efficient Separation of Trivalent Minor Actinides by a Layered Metal Sulfide ($KInSn_2S_6$) from Acidic Radioactive Waste. *J. Am. Chem. Soc.* **2017**, *139*, 16494−16497.

(8) Mei, D.; Yin, W.; Feng, K.; Lin, Z.; Bai, L.; Yao, J.; Wu, Y. $LiGaGe_2Se_6$: A New IR Nonlinear Optical Material with Low Melting Point. *Inorg. Chem.* **2012**, *51*, 1035−1040.

(9) Mei, D.; Zhang, S.; Liang, F.; Zhao, S.; Jiang, J.; Zhong, J.; Lin, Z.; Wu, Y. $LiGaGe_2S_6$: A Chalcogenide with Good Infrared Nonlinear Optical Performance and Low Melting Point. *Inorg. Chem.* **2017**, *56*, 13267−13273.

(10) Kim, Y.; Seo, I.-s.; Martin, S. W.; Baek, J.; Shiv Halasyamani, P.; Arumugam, N.; Steinfink, H. Characterization of New Infrared Nonlinear Optical Material with High Laser Damage Threshold, Li2Ga2GeS6. *Chem. Mater.* **2008**, *20*, 6048−6052.

(11) Yelisseyev, A. P.; Isaenko, L. I.; Krinitsin, P.; Liang, F.; Goloshumova, A. A.; Naumov, D. Y.; Lin, Z. Crystal Growth, Structure, and Optical Properties of $LiGaGe_2Se_6$. *Inorg. Chem.* **2016**, *55*, 8672−8680.

(12) Li, S.-F.; Liu, B.-W.; Zhang, M.-J.; Fan, Y.-H.; Zeng, H.-Y.; Guo, G.-C. Syntheses, Structures, and Nonlinear Optical Properties of Two Sulfides $Na_2In_2MS_6$ (M = Si, Ge). *Inorg. Chem.* **2016**, *55*, 1480−1485.

(13) Yin, W.; Feng, K.; Hao, W.; Yao, J.; Wu, Y. Synthesis, Structure, and Properties of $Li_2In_2MQ_6$ (M = Si, Ge; Q = S, Se): A New Series of IR Nonlinear Optical Materials. *Inorg. Chem.* **2012**, *51*, 5839−5843.

(14) Yohannan, J. P.; Vidyasagar, K. Syntheses and structural characterization of non-centrosymmetric $Na_2M_2M'S_6$ (M, M′ = Ga, In, Si, Ge, Sn, Zn, Cd) sulfides. *J. Solid State Chem.* **2016**, *238*, 147−155.

(15) Yohannan, J. P.; Vidyasagar, K. Syntheses, structural variants and characterization of $AInM'S_4$ (A = alkali metals, Tl; M′ = Ge, Sn) compounds; facile ion-exchange reactions of layered $NaInSnS_4$ and $KInSnS_4$ compounds. *J. Solid State Chem.* **2016**, *238*, 291−302.

(16) Zhou, M.; Li, C.; Li, X.; Yao, J.; Wu, Y. $K_2Sn_2ZnSe_6$, $Na_2Ge_2ZnSe_6$, and $Na_2In_2GeSe_6$: a new series of quaternary selenides with intriguing structural diversity and nonlinear optical properties. *Dalton Trans.* **2016**, *45*, 7627−7633.

(17) Li, S. F.; Yan, D. Synthesis, crystal structure and physical properties of a new chalcogenides $Rb_3Ga_3Ge_7S_{20}$. *J. Solid State Chem.* **2021**, *296*, 121945.

(18) Pogu, A.; Vidyasagar, K. Syntheses, structural variants and characterization of $A_2ZnSn_3S_8$ (A = Cs, Rb) and $A_2CdSn_3S_8$ (A = Cs, Rb, K, Na) compounds. *J. Solid State Chem.* **2020**, *291*, 121647.
(19) Parasyuk, O. V.; Babizhetskyy, V. S.; Khyzhun, O. Y.; Levytskyy, V. O.; Kityk, I. V.; Myronchuk, G. L.; Tsisar, O. V.; Piskach, L. V.; Jedryka, J.; Maciag, A.; Piasecki, M. Novel Quaternary $TlGaSn_2Se_6$ Single Crystal as Promising Material for Laser Operated Infrared Nonlinear Optical Modulators. *Crystals* **2017**, *7*, 341.
(20) Vu, T. V.; Lavrentyev, A. A.; Gabrelian, B. V.; Parasyuk, O. V.; Khyzhun, O. Y. $TlInGe_2S_6$, A Prospective Nonlinear Optical Material: First-Principles DFT Calculations of the Electronic Structure and Optical Properties. *J. Electron. Mater.* **2018**, *47*, 5525−5536.
(21) Vu, T. V.; Lavrentyev, A. A.; Gabrelian, B. V.; Parasyuk, O. V.; Khyzhun, O. Y. First-principles DFT calculations of the electronic structure and optical properties of $TlInGe_2Se_6$, a prospective NLO material. *Mat. Chem. Phys.* **2018**, *219*, 162−174.
(22) Vu, T. V.; Lavrentyev, A. A.; Gabrelian, B. V.; Tong, H. D.; Parasyuk, O. V.; Khyzhun, O. Y. Electronic band structure and basic optical constants of $TlGaSn_2Se_6$, a promising NLO semiconductor: First-principles calculations under DFT framework. *Optik* **2019**, *181*, 673−685.
(23) Al-Bloushi, M.; Davaasuren, B.; Emwas, A.-H.; Rothenberger, A. Synthesis and Characterization of the Quaternary Thioaluminogermanates $A(AlS_2)(GeS_2)$ (A = Na, K). *Z. Anorg. Allg. Chem.* **2015**, *641*, 1352−1356.
(24) Kumari, A.; Vidyasagar, K. Solid-state synthesis, structural variants and transformation of three-dimensional sulfides, $AGaSnS_4$ (A = Na, K, Rb, Cs, Tl) and $Na_{1.263}Ga_{1.263}Sn_{0.737}S_4$. *J. Solid State Chem.* **2007**, *180*, 2013−2019.
(25) Ward, M. D.; Pozzi, E. A.; Van Duyne, R. P.; Ibers, J. A. Syntheses, structures, and optical properties of the indium/germanium selenides $Cs_4In_8GeSe_{16}$, $CsInSe_2$, and $CsInGeSe_4$. *J. Solid State Chem.* **2014**, *212*, 191−196.
(26) Azimi, H.; Hou, Y.; Brabec, C. J. Towards low-cost, environmentally friendly printed chalcopyrite and kesterite solar cells. *Energy Environ. Sci.* **2014**, *7*, 1829−1849.
(27) Giraldo, S.; Jehl, Z.; Placidi, M.; Izquierdo-Roca, V.; Pérez-Rodríguez, A.; Saucedo, E. Progress and Perspectives of Thin Film Kesterite Photovoltaic Technology: A Critical Review. *Adv. Mater.* **2019**, *31*, 1806692.
(28) He, M.; Yan, C.; Li, J.; Suryawanshi, M. P.; Kim, J.; Green, M. A.; Hao, X. Kesterite Solar Cells: Insights into Current Strategies and Challenges. *Adv. Sci.* **2021**, *8*, 2004313.
(29) Fard, Z. H.; Malliakas, C. D.; Mertz, J. L.; Kanatzidis, M. G. Direct Extraction of Ag^+ and Hg^{2+} from Cyanide Complexes and Mode of Binding by the Layered $K_2MgSn_2S_6$ (KMS-2). *Chem. Mater.* **2015**, *27*, 1925−1928.
(30) Manos, M. J.; Ding, N.; Kanatzidis, M. G. Layered metal sulfides: Exceptionally selective agents for radioactive strontium removal. *Proc. Natl. Acad. Sci. U.S.A.* **2008**, *105*, 3696−3699.
(31) Manos, M. J.; Kanatzidis, M. G. Highly Efficient and Rapid Cs^+ Uptake by the Layered Metal Sulfide $K_{2x}Mn_xSn_{3-x}S_6$ (KMS-1). *J. Am. Chem. Soc.* **2009**, *131*, 6599−6607.
(32) Manos, M. J.; Kanatzidis, M. G. Layered Metal Sulfides Capture Uranium from Seawater. *J. Am. Chem. Soc.* **2012**, *134*, 16441−16446.
(33) Manos, M. J.; Petkov, V. G.; Kanatzidis, M. G. $H_{2x}Mn_xSn_{3-x}S_6$ (x=0.11-0.25): A Novel Reusable Sorbent for Highly Specific Mercury Capture Under Extreme pH Conditions. *Adv. Funct. Mater.* **2009**, *19*, 1087−1092.
(34) Mertz, J. L.; Fard, Z. H.; Malliakas, C. D.; Manos, M. J.; Kanatzidis, M. G. Selective Removal of Cs^+, Sr^{2+}, and Ni^{2+} by $K_{2x}Mg_xSn_{3-x}S_6$ (x=0.5-1) (KMS-2) Relevant to Nuclear Waste Remediation. *Chem. Mater.* **2013**, *25*, 2116−2127.
(35) Neeway, J. J.; Asmussen, R. M.; Lawter, A. R.; Bowden, M. E.; Lukens, W. W.; Sarma, D.; Riley, B. J.; Kanatzidis, M. G.; Qafoku, N. P. Removal of TcO_4^- from Representative Nuclear Waste Streams with Layered Potassium Metal Sulfide Materials. *Chem. Mater.* **2016**, *28*, 3976−3983.
(36) Xu, L.; Xu, C.; Bao, H. L.; Spanopoulos, I.; Ke, W. J.; Dong, X.; Xiao, C. L.; Kanatzidis, M. G. Selective Capture Mechanism of Radioactive Thorium from Highly Acidic Solution by a Layered Metal Sulfide. *ACS Appl. Mater. Interfaces* **2021**, *13*, 37298−37305.
(37) Manos, M. J.; Kanatzidis, M. G. Metal sulfide ion exchangers: superior sorbents for the capture of toxic and nuclear waste-related metal ions. *Chem. Sci.* **2016**, *7*, 4804−4824.
(38) Bouchenafa, M.; Sidoumou, M.; Halit, M.; Benmakhlouf, A.; Bouhemadou, A.; Maabed, S.; Bentabet, A.; Bin-Omran, S. Theoretical investigation of the structural, elastic, electronic and optical properties of the ternary indium sulfide layered structures $AInS_2$ (A = K, Rb and Cs). *Solid State Sci.* **2018**, *76*, 74−84.
(39) Sheldrick, G. M. *SHELXL-97—Program for Structures Refinement*; University of Göttingen, 1997.
(40) Spek, A. Single-crystal structure validation with the program PLATON. *J. Appl. Crystallogr.* **2003**, *36*, 7−13.
(41) Kubelks, P.; Munk, E. Ein Beitrag zur Optik der Farbanstriche. *Z. Tech. Phys.* **1931**, *12*, 593−601.
(42) Kresse, G.; Furthmüller, J. Efficient iterative schemes for ab initio total-energy calculations using a plane-wave basis set. *Phys. Rev. B: Condens. Matter Mater. Phys.* **1996**, *54*, 11169−11186.
(43) Tran, F.; Blaha, P. Accurate Band Gaps of Semiconductors and Insulators with a Semilocal Exchange-Correlation Potential. *Phys. Rev. Lett.* **2009**, *102*, 226401.
(44) Becke, A. D.; Johnson, E. R. A simple effective potential for exchange. *J. Chem. Phys.* **2006**, *124*, 221101.
(45) Kresse, G.; Furthmüller, J. Efficient iterative schemes for ab initio total-energy calculations using a plane-wave basis set. *Phys. Rev. B: Condens. Matter Mater. Phys.* **1996**, *54*, 11169−11186.
(46) Shannon, R. Revised effective ionic radii and systematic studies of interatomic distances in halides and chalcogenides. *Acta Crystallogr. Sect. A Cryst. Phys. Diffr. Theor. Gen. Crystallogr.* **1976**, *32*, 751−767.
(47) Friedrich, D.; Schlosser, M.; Pfitzner, A. Synthesis, Crystal Structure, and Physical Properties of Two Polymorphs of $CsGaSe_2$, and High-Temperature X-ray Diffraction Study of the Phase Transition Kinetics. *Cryst. Growth Des.* **2016**, *16*, 3983−3992.
(48) Friedrich, D.; Schlosser, M.; Pfitzner, A. Synthesis and Structural Characterization of the layered Selenogallate $RbGaSe_2$. *Z. Anorg. Allg. Chem.* **2017**, *643*, 1589−1592.
(49) Friedrich, D.; Schlosser, M.; Weihrich, R.; Pfitzner, A. Polymorphism of $CsGaS_2$ - structural characterization of a new two-dimensional polymorph and study of the phase-transition kinetics. *Inorg. Chem. Front.* **2017**, *4*, 393−400.
(50) He, J.; Zhang, X.; Guo, P.; Cheng, Y.; Zheng, C.; Huang, F. Synthesis, structure, and optical properties of $K_{2.4}Ga_{2.4}M_{1.6}Q_8$ (M = Si, Ge; Q = S, Se) crystals and glasses. *RSC Adv.* **2016**, *6*, 76789−76794.
(51) Liu, Q.-Q.; Liu, X.; Chen, L.; Wu, L.-M. $AGaSnS_4$ (A = Rb, Cs): Three sulfides and their structure diversity. *J. Solid State Chem.* **2020**, *285*, 121233.
(52) Axtell, E. A.; Park, Y.; Chondroudis, K.; Kanatzidis, M. G. Incorporation of A_2Q into HgQ and dimensional reduction to $A_2Hg_3Q_4$ and $A_2Hg_6Q_7$ (A= K, Rb, Cs; Q= S, Se). Access of Li ions in $A_2Hg_6Q_7$ through topotactic ion-exchange. *J. Am. Chem. Soc.* **1998**, *120*, 124−136.
(53) Axtell, E. A., III; Liao, J. H.; Pikramenou, Z.; Kanatzidis, M. G. Dimensional reduction in II-VI materials: $A_2Cd_3Q_4$ (A= K, Q= S, Se, Te; A= Rb, Q= S, Se), novel ternary low-dimensional cadmium chalcogenides produced by incorporation of A_2Q in CdQ. *Chem. - Eur. J.* **1996**, *2*, 656−666.

https://doi.org/10.1021/acs.inorgchem.2c02157
Inorg. Chem. 2022, 61, 13525−13531